Hydrofracture in Weber Sandstone at High Confining Pressure and Differential Stress

D. LOCKNER AND J. D. BYERLEE

U.S. Geological Survey, Menlo Park, California 94205

Acoustic emission monitored during the hydraulic fracturing of two intact samples of Weber sandstone was used to determine the location and orientation of macroscopic fracture planes caused by the fracturing process. The locations of microfractures that were determined from the acoustic emission data corresponded closely with observed fractures. Pore fluid was injected into the two samples at different rates (3.3×10^{-5} cc/s and 3.3×10^{-4} cc/s) until failure occurred. The sample injected at the slower rate failed in shear, whereas the sample injected at the faster rate failed in tension. Both samples were subjected to 1000-bars confining pressure and 4000-bars differential stress. To further study how tension and shear failure depend on pore fluid injection rate and differential stress, a series of 16 hydraulic fracture experiments were run on smaller 2.54-cm-diameter samples without monitoring acoustic emission. It was found that over a wide range of stresses, either shear or tension failure could be produced simply by varying the rate at which fluid was injected into the sample. A theoretical model was developed to calculate the pore pressure distribution in the samples as a function of time, borehole pressure, and differential stress. The model was used to relate the failure mechanism (tension or shear failure) to the pore pressure distribution in each sample by analysis that required knowledge of the porosity and permeability of Weber sandstone. To supply the input data necessary for the numerical model, a series of permeability measurements were conducted. These measurements show that permeability is dependent upon effective pressure and differential stress. The principal goals of these experiments were to determine whether acoustic emission could be used to locate hydraulic fractures and to study the factors which control hydraulic fracture initiation, either in tension or in shear.

INTRODUCTION

Hydraulic fracturing is a technique of great use in augmenting production of tight oil- and gas-bearing rocks as well as in the development of artificial geothermal reservoirs. At the present time much effort is being directed toward the development of ways to locate fracture planes resulting from hydraulic fracturing. One such technique is the monitoring of acoustic emission generated during the fracturing process. *Shuck and Keech* [1975] have reported the results of a hydraulic fracture experiment conducted by the Morgantown Energy Research Center. In their preliminary analysis they had not yet identified any acoustic signals that could be used to locate fracture, presumably due to the high attenuation and low amplitude of the acoustic waves generated by crack growth. *Woullet and Power* [1975] reported a similar experiment conducted by the El Paso Natural Gas Company. In this experiment researchers were again unable to detect acoustic emission above the background noise level. Despite these early discouraging results, further field experiments have been proposed using more sophisticated equipment for detection of acoustic emission.

Because of the importance of determining the feasibility of using acoustic emission to locate hydraulic fractures we have performed similar experiments in the laboratory. In these experiments we have attempted to duplicate some of the conditions encountered in the field. Samples were subjected to confining pressure and differential stress to duplicate hydrostatic loading and deviatory tectonic stresses. They were then fractured by injecting oil into a drill hole oriented parallel to the most compressive principal stress. Piezoelectric transducers attached to the samples monitored the acoustic emission generated during the fracturing process in an attempt to locate the fracture planes formed during failure.

In the literature on hydraulic fracture experiments it is generally assumed that a crack will initiate when the tensile stress at the borehole wall exceeds the tensile strength of the rock. It is possible, however, that in regions under tectonic shear stress, shear failure could be induced in the rock about the borehole at much lower fluid pressures than would be required to produce tension cracks, simply by lowering the effective pressure (confining pressure minus pore pressure) to the point where the shear strength of the rock is exceeded. *Byerlee* [1975] showed that the compressional strength of Weber sandstone depends on effective pressure and differential stress. This suggested that a sample subjected to a given confining pressure and differential stress could be made to fail in shear or tension simply by controlling the pore pressure. One way of testing this hypothesis would be to vary the pore fluid injection rate. At slow injection rates the pore fluid would have time to diffuse into the sample and lower the effective pressure, whereas at fast injection rates a steep pore pressure gradient would develop near the borehole. If fluid were injected fast enough, even though the shear strength of the rock near the borehole would be exceeded, the load on the sample would be supported by the surrounding rock in which the pore pressure was still low. In this way, shear failure of the sample would not occur and instead, a tension crack would form when the tensile strength of the rock near the borehole was exceeded. To test this hypothesis, a series of 16 experiments was conducted on samples of Weber sandstone at differential stresses ranging from 1 to 4 kbar (10 kbar = 1 GPa) and at fluid injection rates varying by 3 orders of magnitude.

It was assumed that the failure mechanisms (shear or tension) observed for different injection rates would be controlled by the pore pressure distribution in each sample at the time of failure. To calculate the pore pressure distributions for the different runs, a theoretical model based on the equation for radial flow in a porous medium was developed. The model used a finite differencing method in a computer program to calculate the time dependent radial pressure distribution in each experiment.

In the remainder of this paper the experiments are discussed in the following way. First, the experimental method is de-

Paper number 7B0145.

scribed for two experiments in which acoustic emission from the sample was monitored and for 16 experiments in which acoustic emission was not monitored. This is followed by a brief formulation of the numerical model used to calculate the pore pressure distribution in the samples. Next we present the results of the location of microfractures occurring during failure in the two acoustic emission experiments. In the following section we show how failure mode (shear or tension) is related to differential stress and pore fluid injection rate. Finally, we discuss some of the implications that these results have on in situ hydraulic fracturing.

EXPERIMENTAL METHOD FOR MONITORING ACOUSTIC EMISSION

A core of the Pennsylvanian Weber sandstone from the subsurface of the Rangely oil field in northwest Colorado was sampled for study. Two cylindrical samples of the rock, herein termed 'Weber sandstone,' 19.05 cm long and 7.62 cm in diameter, were prepared for the acoustic emission experiments. These large samples were used to increase the relative accuracy of the location of microseismic events. A 0.16-cm-diameter hole was drilled down the axis of each sample for injection of fracturing fluid (Figure 1). Copper gaskets 0.0025 cm thick were placed between the ends of the samples and the anvils to prevent pore fluid from leaking out of the drill hole along this surface. Each sample was placed in a polyurethane sleeve to isolate it from the confining fluid and had six piezoelectric transducers cemented to its surface to monitor the high-frequency acoustic emission generated during failure. After being mounted in a pressure vessel, a confining pressure of 1000 bars was applied to each sample and held constant throughout the experiments. An additional axial load of 4 kbar was then applied to each sample. After a period of primary creep (<30 min) caused by the initial loading, the samples were maintained at constant axial strain, so that, as in nature, shear stress would decrease as the rock moved along faults. Axial displacement was measured with a displacement transducer mounted on the piston, outside of the pressure vessel.

When the primary creep and the acoustic emission caused by the initial loading had ceased, oil was injected into the drill hole in each sample by a constant rate pump. This was done by initially raising the borehole pressure to 40 bars and then starting the pump, and allowing the pressure to increase as the pump advanced. In experiment 1, pore fluid was injected at a rate of 3.3×10^{-5} cc/s, while in experiment 2 it was injected at 3.3×10^{-4} cc/s. During both experiments the outputs of the piezoelectric transducers attached to the samples were amplified and fed into an electronic timing system. For a description of this system and the technique used to locate the microfractures, refer to *Byerlee and Lockner* [1977].

METHOD FOR STUDYING TENSION VERSUS SHEAR FAILURE

To further study the relative dependence of tension and shear failure on fluid injection rate a series of experiments was performed on samples of Weber sandstone without monitoring acoustic emission. For this series, smaller samples (2.54-cm diameter by 6.35 cm long) were prepared and mounted in the same fashion as the samples used in the acoustic emission experiments. Confining pressure for all small-sample experiments was 1000 bars. Differential stress was held constant in each experiment at a value between 1 and 4 kbar, and injection rates ranged from 3.3×10^{-6} cc/s to 3.3×10^{-3} cc/s. Pore fluid was injected into the borehole until the sample failed in either shear or tension. The experiments performed on samples that failed in tension were ended after injection pressure dropped to the confining pressure, indicating that a fracture had formed that allowed the injection fluid to reach the jacket. Such fractures could be seen in the samples by visual inspection. The experiments in which the samples failed in shear were ended when axial strain of at least 5% had been reached accompanied by a decrease in the injection pressure.

In summary, the key elements of the experimental method are as follows. Throughout all the experiments, confining pressure was held constant at 1000 bars. In the two acoustic emission experiments a differential stress of 4 kbar was initially maintained during primary creep. Both samples were then held at constant strain, allowing differential stress to drop as failure

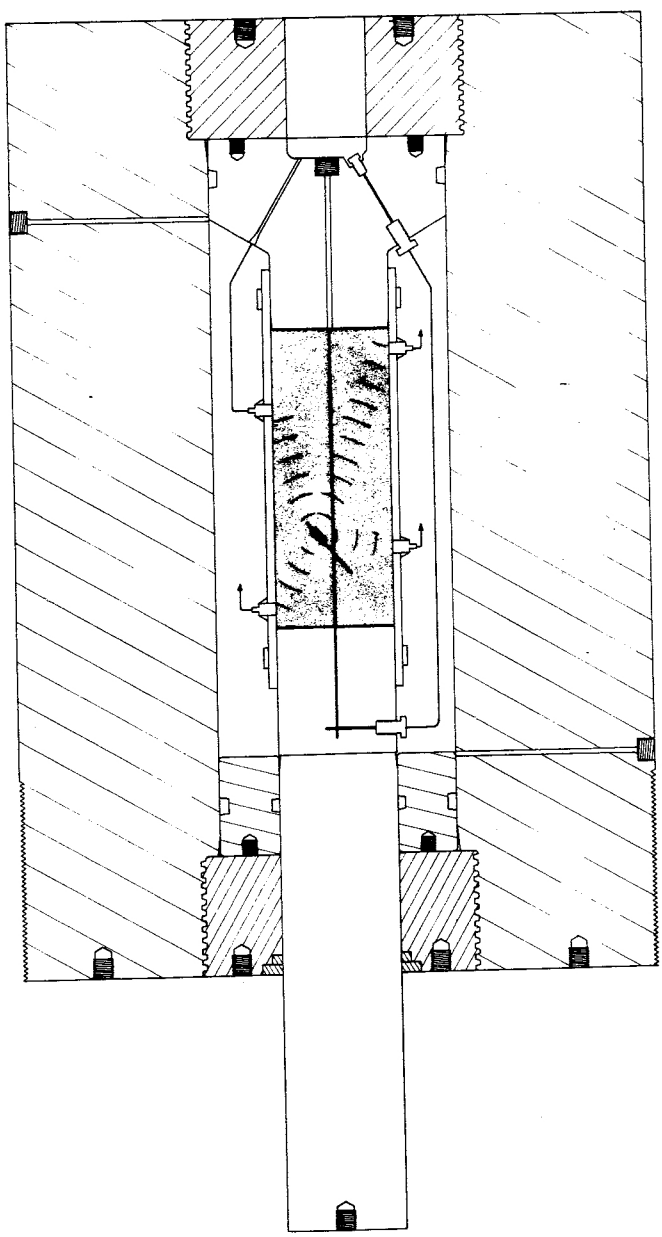

Fig. 1. Experimental setup of acoustic emission experiments showing cross section of sample mounted in pressure vessel. Pore fluid is injected into borehole. Acoustic signals are monitored by transducers mounted on sides of sample.

occurred. In experiment 1, pore fluid was injected at a rate of 3.3×10^{-5} cc/s until failure, whereas in experiment 2 it was injected at a rate of 3.3×10^{-4} cc/s. The principal difference between the two acoustic emission experiments, then, was that in the second, pore fluid was injected at a rate 10 times as fast as in the first. The series of 16 experiments using small samples without monitoring acoustic emission was conducted at constant confining pressure and differential stress and at fluid injection rates that ranged over 3 orders of magnitude.

Formulation of Numerical Pore Pressure Model

We assume that the failure mode was related to the pore pressure distribution within the samples. Since we were able to measure only the fluid pressure at the borehole, a numerical model was used to calculate the radial distribution of pore pressure as a function of borehole pressure. A computer program was developed using a finite difference scheme to calculate the pore pressure distribution from the equation for radial flow in a porous medium:

$$\frac{\partial^2 p}{\partial r^2} + \frac{1}{r}\frac{\partial p}{\partial r} + (c+\beta)\left(\frac{\partial p}{\partial r}\right)^2 = \frac{\mu}{k}\phi c \frac{\partial p}{\partial t} \qquad (1)$$

which was adapted from *Mathews and Russel* [1967]. In (1) the compressibility is given by $c = 1/\rho\ \partial\rho/\partial p$, where ρ is density, μ is dynamic viscosity, k is permeability, ϕ is porosity, and the pressure dependence of permeability and viscosity is given by

$$\beta = \left(\frac{k}{\mu}\right)^{-1}\frac{\partial}{\partial p}\left(\frac{k}{\mu}\right) \qquad (2)$$

To simplify computations, the compressibility of the pore fluid (Shell Tellus oil 15 [*Shell International Petroleum*, 1967]) was assumed to be constant. The compressibility and the dependence of viscosity on pressure were taken from the Shell tables [*Shell International Petroleum*, 1967]. Measurements conducted on the Weber sandstone gave an average porosity of 5.5%.

Because permeability depends on the stress conditions of the sample, a series of permeability measurements were conducted on 2.54-cm-diameter samples of Weber sandstone at different-

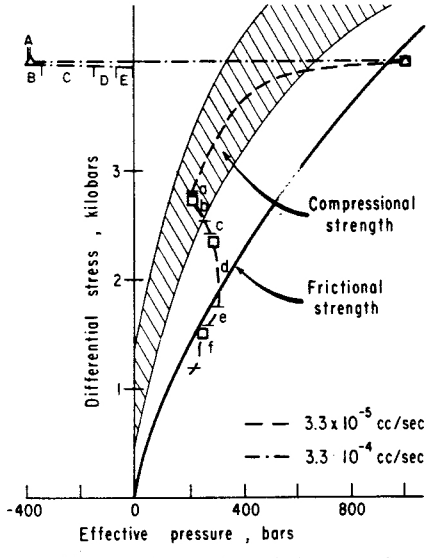

Fig. 2. Stress history of acoustic emission experiments 1 and 2. Letters show the time intervals in the experiments for which microfracture locations are plotted in Figures 3, 4, and 5.

ial stresses ranging from 0 to 4 kbar and effective pressure ranging from 200 to 900 bars. Because of the low permeability of the Weber, argon gas was used as a pore fluid. Permeability was measured by means of a pulse decay method employed by *Zoback* [1975] similar to that used by *Brace et al.* [1968] and *Sanyal et al.* [1972]. Using this technique, permeabilities as low as a few nanodarcies (nda) could be measured.

Normally, in fluid diffusion problems it is assumed that pressure gradients are small enough that the second-order term $(\partial p/\partial r)^2$ can be neglected. In this case, (1) reduces to the familiar diffusion equation. *Yilmaz and Nur* [1971] have shown that for flow conditions involving large pressure gradients the second-order term dominates the flow equation, causing a steep pressure front to propagate through the medium. In our analysis it was found that the second-order term does become important in the case of high fluid injection rates. As a result, the $(\partial p/\partial r)^2$ was retained in the analysis. At slow injection rates this term becomes negligible and (1) behaves as the standard diffusion equation. The finite difference form of (1) becomes

$$p_i' = p_i + \frac{k_i}{\mu_i}\frac{\Delta t}{\phi c}\left[\frac{(p_{i+1} + p_{i-1} - 2p_i)}{(\Delta r)^2} + \frac{1}{r}\frac{(p_{i+1} - p_{i-1})}{2\Delta r} + (c+\beta)\left(\frac{p_{i+1} - p_{i-1}}{2\Delta r}\right)^2\right] \qquad (3)$$

where the subscripts refer to the radial coordinate and p_i' is the pressure in the ith cell at time $t + \Delta t$. The parameter β in (3) was estimated from the permeability data and from the viscosity of the Tellus 15 oil [*Shell International Petroleum*, 1967].

Results of Microfracture Locations

For the two acoustic emission experiments, differential stress is plotted in relation to effective pressure σ_e, defined as confining pressure minus injection pressure (Figure 2). For approximately 6 days, sample 1 showed a continuous decrease in differential stress from 4 to 2.67 kbar as the injection pressure increased. During this period the stress that the sample supported followed the compressional strength curve of Weber sandstone [*Byerlee*, 1975]. When the effective stress near the borehole had dropped to 220 bars, the differential stress suddenly dropped in two steps to 1.75 kbar as macroscopic faults developed in the sample. It then stabilized at a point on the frictional strength curve as determined by *Byerlee* [1975] and moved along this curve until the differential stress had dropped to 1.5 kbar, where the stress again dropped abruptly as the sample slipped along shear faults. The differential stress then gradually dropped to 1.1 kbar, at which point the experiment was ended.

During this experiment the acoustic emission rate varied widely. As the initial loading of the sample took place, microseismic events occurred at a faster rate than could be recorded by our equipment ($\sim 5 \times 10^5$ events per hour). As primary creep ended (when there was no longer any change in axial displacement), this activity dropped off to a rate of about 2 events per hour. Computer analysis which calculated the locations of these early events showed that during the loading of the sample, microfracture activity was spread uniformly throughout the sample. The acoustic emission rate remained low for more than 6 days and showed no grouping of events in localized areas of the sample. Some 10 min before the first sudden stress drop, however, the activity sharply increased to a

rate of more than 10^6 events per hour. Each successive stress drop (indicated by the squares in Figure 2) was preceded by a sudden increase followed by a gradual tapering off of the acoustic emission rate.

The locations of the microseismic events accompanying each successive stress drop were concentrated along distinct planes that show a one-to-one correspondence to easily identified fault planes in the sample. Figure 3 shows the microfracture locations obtained from the acoustic emission data. For each time period, three views of the sample are given (one top view and two side views 90° apart). Because of the amount of data involved we chose to display it in terms of density of events per unit area. In each figure all of the microseismic events are projected onto a plane. The projections are then divided up by grids with a unit area of 0.1 cm^2, and the number of events in each grid cell is tallied. These densities are then contoured, resulting in the plots shown in Figure 3. The heavy lines in the figure represent the projections of observed fault planes. Each figure has been rotated to give the sharpest resolution of clusters of events. Both the locations and the strikes of the clusters of microseismic events are in close agreement with those of observed fault planes. This shows that acoustic emission data can be used to determine fault plane location and orientation.

In experiment 2, pore fluid was injected at a rate 10 times as fast as that in experiment 1. Injection pressure rose to 1400 bars, at which point a tension fracture formed parallel to the maximum principal stress. The borehole pressure then dropped to 1015 bars as pore fluid escaped through the tension fracture to the surface of the sample. It should be kept in mind that the effective pressure plotted in Figure 2 is measured at the bore wall. With lower pore pressure near the surface of the sample, the outer portion of the sample is at much higher effective pressure. During the entire experiment 2 no measurable stress drop occurred. At failure, two vertical fractures were formed on opposite sides of the sample with orientations as shown by the heavy lines in the top view of Figure 4. The surface expression of the fractures is shown in the side views of these figures.

During the initial loading of the sample in experiment 2, recorded acoustic emission events occurred at a rate greater than 10^5 per hour. These events were distributed randomly throughout the sample, as was true in experiment 1. Similarly, 30 min after the stress had been applied the detectable acoustic emission had dropped off to less than 40 events per hour. After 3 hours, the detectable acoustic emission ceased until just prior to failure (a period of approximately 2½ hours).

In less than 2 min the acoustic emission rate jumped from zero to more than 10^6 events per hour as the fractures formed, then dropped off gradually to a rate of 10^4 events per hour after 40 min.

The first microseisms to occur before failure were located near the borehole in the center of the fracture zone (Figure 4). The center of microseismic activity then moved along the fracture zone. In Figure 5, microfracture locations are projected onto the fracture plane, and the radial distribution of these events is plotted relative to time. The radial distribution (Figure 5) shows that for about the first minute the activity occurred in a region about one side of the borehole; the crack then became unstable and quickly propagated to the surface of

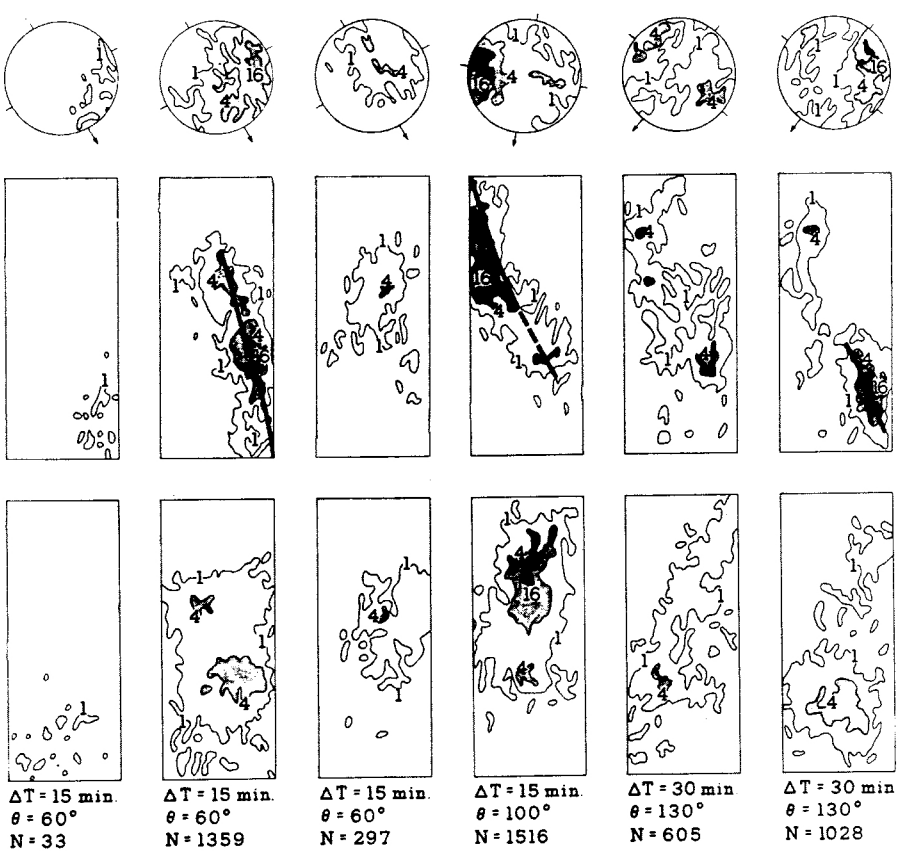

Fig. 3. Locations of microfractures from arrival time data for sample 1. Densities of events per unit area are plotted. Heavy lines are projections of observed faults.

the sample. At this time, microfractures began to form on the other side of the borehole and rapidly progressed to the surface. Locations of microfractures (Figure 4) show that the later microseisms occurred in an increasingly diffuse region about the fracture surface, possibly as a result of pore fluid penetrating into this region. Figures 4 and 5 show that tension fractures produced in experiment 2 were located successfully by analysis of microfractures occurring during failure.

DEPENDENCE OF FAILURE MODE ON STRESS AND PORE PRESSURE

A series of 16 hydraulic fracture experiments was performed on 2.54-cm-diameter samples without monitoring acoustic emissions. The breakdown pressures in these experiments are plotted in Figure 6. Despite some scatter in the data that can be explained by the large variation in permeability and compressional strength from sample to sample, overall trends are apparent. At the slowest pumping rates in which the pore fluid is able to diffuse throughout the sample, failure occurs in shear at stresses near the compressional strength curve of the rock. At faster injection rates the samples fail in tension with much lower effective pressure in the region of the borehole. All samples that failed at effective pressure greater than -100 bars, failed in shear, whereas those failing at effective pressure less than -100 bars, failed in tension.

The final experiment in this series was conducted at 1-kbar confining pressure, 1-kbar differential stress, and fluid injection rate of 3.3×10^{-6} cc/s. After 20 days the borehole pressure had leveled off at 1010 bars. The sample showed no axial strain; nor did it show any other signs that it was approaching failure. However, the confining fluid had to be bled off periodically to maintain constant pressure, indicating that pore fluid was permeating through the sample and accumulating beneath the polyurethane jacket. Because the unconfined strength of Weber sandstone is greater than 1 kbar, we conclude that the sample had reached an equilibrium state in which the amount of oil injected into the borehole was equal to the amount leaving the outer surface of the sample. As this represents a steady flow condition, it is a simple matter to calculate the permeability in the sample perpendicular to the maximum principal stress from Darcy's law. Such calculation yields a permeability of 2.0 ± 0.5 microdarcies (μda) for 1-kbar differential stress and 0-kbar effective pressure. Extrapolation of the permeability data from the argon gas measurements would suggest a permeability under these stress conditions closer to 200 nda. This shows that permeability is extremely sensitive to changes in effective pressure σ_e near zero.

This permeability, together with the measurements obtained from the pulse decay method, is plotted in Figure 7. In this figure, permeability at different differential stresses is plotted

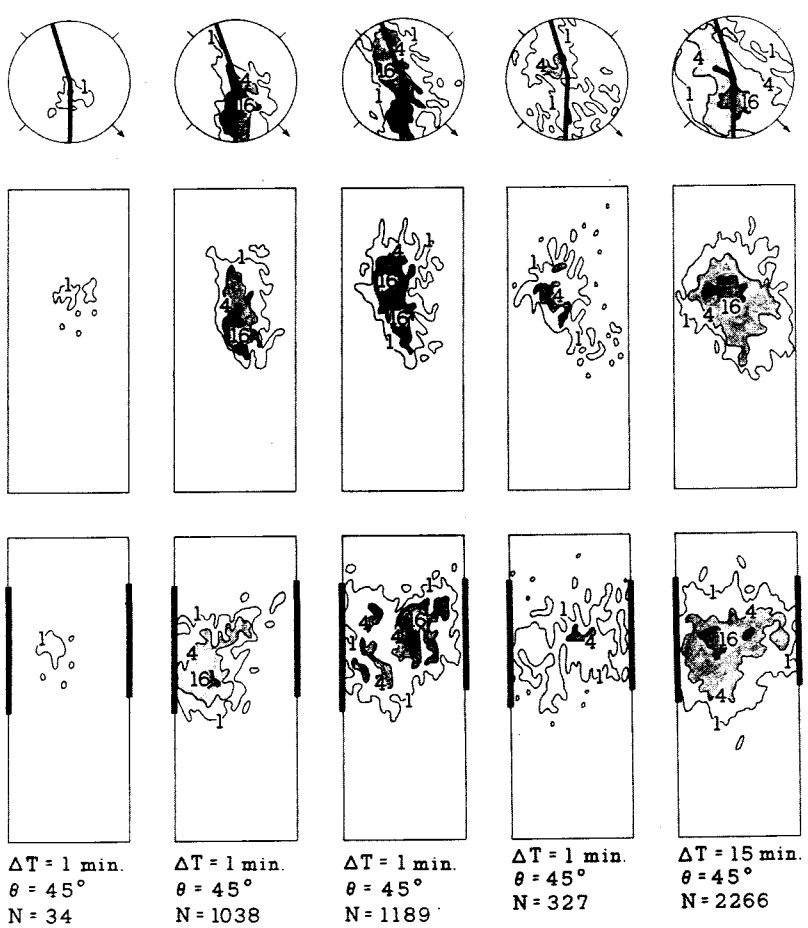

Fig. 4. Locations of microfractures, showing the development of the fracture surface, for sample 2. Densities of events per unit area are plotted. Heavy lines in top view are projections of the fracture surface; in side views they represent surface expression of fracture.

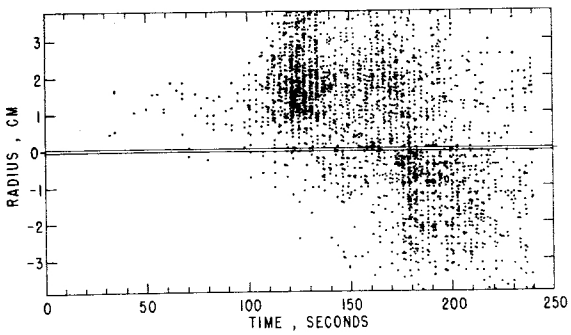

Fig. 5. Plot of the radial distribution of microfractures showing the detailed development of the fracture surface for experiment 2.

as a function of effective pressure. The permeability measured in the pulse decay experiments is for flow parallel to the axis of the sample, whereas calculation of the pore pressure distribution requires knowledge of permeability in the radial directions. At low differential stress, axial and radial permeabilities should be comparable. At high differential stress, where preferential growth of cracks is parallel to the direction of maximum loading, axial permeability should be an upper limit for the radial permeability. The single measurement at zero effective pressure represents the permeability for radial flow obtained from the final hydrofrac experiment. At a given differential stress, permeability decreases with increasing effective pressure, probably as a result of closure of preexisting cracks. The data show that for Weber sandstone, most of the crack closure which contributes to the permeability of the rock occurs between 0- and 200-bars effective pressure.

If effective pressure is held constant and differential stress is increased, the axial permeability first decreases and then increases, a minimum value occurring at about 1-kbar differential stress. One interpretation of this behavior is that with the initial loading of the sample, preexisting cracks in the rock begin to close, causing a decrease in permeability. With continued increase in differential stress, however, the rock begins to dilate as new cracks are opened parallel to its axis, causing an increase in the permeability in this direction.

Because it is impossible to measure permeabilities at stresses once the compressive strength of the rock has been reached, and since it is not clear just how the permeability should behave in this region, the permeability used in the numerical pore pressure model was arbitrarily limited to a maximum of 2 μda. We feel that this is a conservative estimate of the permeability in this region. Because of this constraint the results of the numerical model can be applied quantitatively only to experiments that failed near or below the compressive strength of the rock. For samples that failed in tension at higher breakdown pressures the model can supply a qualitative description of the pore pressure distribution at the time of failure.

The radial pore pressure distribution at failure was calculated by means of the diffusion model for three hydrofrac experiments conducted on samples at 4-kbar differential stress and over a range of injection rates. Results are shown in Figure 8. All three of these samples failed in shear. In addition, the pore pressure distribution was calculated for acoustic emission experiment 1 as shown by the curve in Figure 8. The actual borehole pressure histories from each experiment were used as input to the model. Byerlee has shown that the strength of Weber sandstone is a function of effective pressure. In these experiments as the pore pressure is increased, effective pressure drops until the compressive strength of the rock is reached. (The region in which the compressive strength of Weber will be reached is indicated by the dashed lines.) Although this is a fairly wide region, all of our results suggest that the samples used had strengths near the top of this zone. The samples used in these experiments were chosen for similarity in physical appearance in order to maintain as small a variation between samples as possible. The pressure curves for the three experiments conducted at 4-kbar differential stress (Figure 8) show a systematic increase of the pore pressure gradient with increased pumping rate. A fourth experiment conducted at 4 kbar and at a pumping rate of 3.3×10^{-2} cc/s failed in tension. We were unable to calculate the pore pressure distribution for this experiment because we could not measure the permeability at negative effective pressure. The most reasonable explanation, however, is that at the fast pumping rate the pressure gradient was so large that the tensile strength of the rock near the borehole was exceeded before the shear strength of the outer part of the sample was reached. All of our results are consistent with this interpretation of the mechanism that determined whether a particular sample would fail in shear or tension. When high pressure gradients exist, especially when the permeability rises sharply as the effective pressure approaches zero, a sharp pressure front develops in the sample, moving outward from the borehole. As long as the permeability increases with increasing pore pressure, a steep pressure gradient will tend to develop. The detailed dependence of permeability on pressure will affect only the rate at which the pressure front advances through the sample. Thus the numerical model suggests that quite different pressure distributions exist in samples that fail in tension and samples that fail in shear.

Discussion

The two acoustic emission experiments reported in this paper represent the first successful attempt to trace the detailed growth of fracture planes during hydraulic fracturing by means of the acoustic emission generated during the fracturing process. Even though it is a large jump from laboratory experiments to the field, of the results reported recently, these are the most encouraging. The largest problems in utilizing this technique in the field are the low amplitude and rapid attenuation of the acoustic emission. In our experiments we recorded in the megahertz range to achieve a location accuracy of a millime-

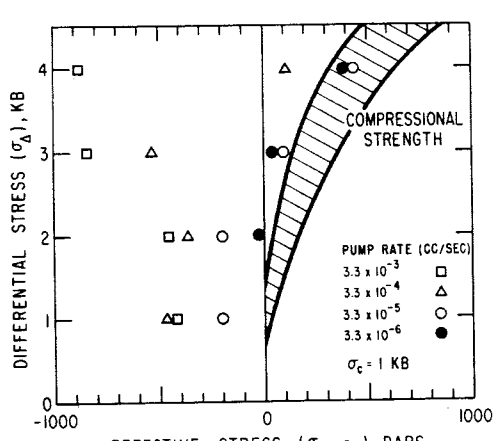

Fig. 6. Plot of differential stress relative to effective pressure at breakdown for 2.54-cm-diameter samples. All samples to the right of −100-bars effective pressure failed in shear; all others failed in tension.

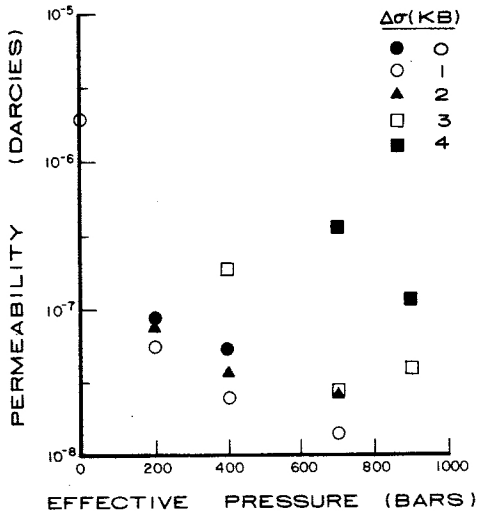

Fig. 7. Permeability measurements on Weber sandstone shown as a function of effective pressure.

ter, a procedure that is, however, neither feasible nor necessary in the field. Attaining accuracies of the order of a few meters would require working at frequencies around 100 Hz. Since seismic records can commonly be read to a millisecond, this should not be an obstacle. Still, at 100 Hz, acoustic signals are rapidly attenuated in the earth. To successfully record the acoustic signals, transducers will need to be placed near the fracture front. By burying the transducers below the highly attenuating surface layer, signal-to-noise ratios could be enhanced. In addition, techniques need to be developed to filter out noise caused by the injection pumps. Such problems are being dealt with by the Morgantown Energy Research group and other workers who are preparing to conduct field experiments on acoustic emission.

A significant feature of the experiments presented here is that with the instrumentation used, acoustic emission was not detected until the onset of failure. Numerical analysis indicates that prior to failure, pore pressure is sufficiently high in a region about the borehole to expect some slippage on grain boundaries and opening of cracks. If this is occurring, the energy released is too little to produce acoustic emission above the threshold level of our equipment. It is possible that the presence of the pore fluid preferentially induces low-energy cracking in the rock. If this is true, it would suggest that the *b* value in the log number relative to log amplitude plot for acoustic emission in dry samples differs from that for hydraulically fractured samples. Preliminary studies of these phenomena, however, show no significant difference in *b* values for dry and wet samples.

Another aspect of interest is the transient stress behavior exhibited by sample 1. Because the axial strain was held constant during this experiment, the differential stress dropped as the sample failed. As is shown in Figure 2, the sample followed the compressive strength curve during the 6 days that it remained intact. With the formation of throughgoing faults in the sample the stress dropped to the frictional strength curve. To explain this phenomenon, consider the small-scale response of the rock to high differential stress. As the pore pressure increases, bringing the rock close to its compressive strength, small fractures will open throughout the rock, causing small-scale dilatant regions. The development of such dilatant regions has the effect of reducing the local stress concentrations. By means of this process the rock will gradually convert elastic strain to permanent deformation as it shears uniformly on microscopic shear planes distributed throughout the sample. At some point this process becomes unstable, causing the formation of throughgoing faults in a manner similar to that found by *Wawersik and Brace* [1971] in creep experiments. It is not clear in experiment 1 why this instability occurred when it did, but in a qualitative way it is reasonable to assume that it is related to the coalescing of the microfractures when their density has increased to the point that they begin to influence each other.

Once a throughgoing fault is formed, it is not surprising that the rock should be able to support only a shear stress on the fault surface equal to the frictional strength of the rock. In experiment 1 the first fault to form bottomed out on one of the anvils, leaving a column of unfractured rock still supporting part of the load until a second fault formed. At this point the stress dropped to the frictional strength curve. It would be interesting to perform this same experiment on a dry sample to see what effect pore fluid had in this process.

In sample 2 the first microfractures to occur prior to the drop in injection pressure are in a region bounded on one side by the borehole and extending 2 cm toward the surface (Figure 5). The fracture remained stable at this length for about 1 min before accelerating toward the surface. At the same time a second tension crack developed on the other side of the borehole and propagated unstably to the surface. Theoretical calculation of the pore pressure distribution at failure indicates that a large pore pressure gradient existed about midway between the center of the sample and the outer surface. If this were the case, the abrupt change in effective pressure that would result from such a gradient could inhibit crack propagation in this region, resulting in the two-stage crack growth observed in Figure 5.

Theoretical calculations carried out by *Clifton et al.* [1974, 1976] suggest an alternative explanation for this phenomenon. In their analysis of the stress intensity factor for thick-walled vessels they showed that for a sample with the ratio (sample diameter)/(borehole diameter) ≥ 10, there exists a region in which double-extension cracks will grow stably. For the size

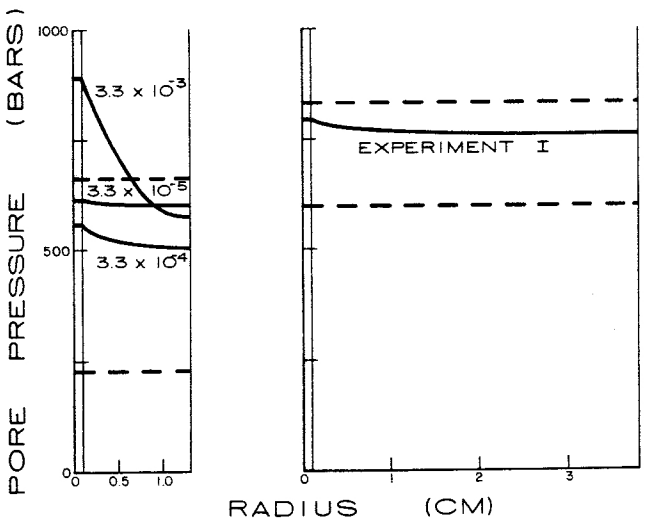

Fig. 8. Theoretical calculation of radial pore pressure distribution from numerical model. At the left are plotted pressure curves for three samples conducted at 4-kbar differential stress. At the right is a plot of the pore pressure in the larger sample used in acoustic emission experiment 1. All of these samples failed in shear.

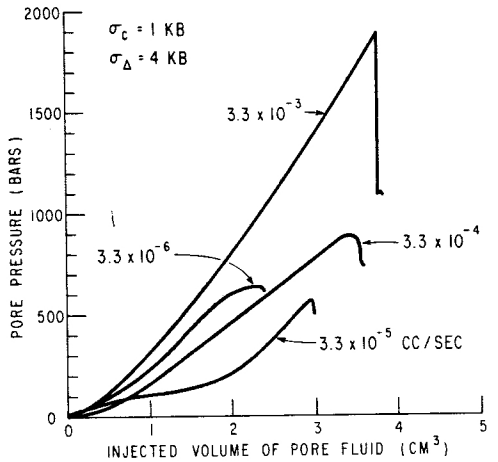

Fig. 9. Borehole pressure curves for four experiments conducted at 1-kbar confining pressure and 4-kbar differential stress.

sample used in experiment 2 a tension crack would grow stably until it had extended to nearly half the sample radius. Once it had reached this length, however, it would grow unstably to the sample surface. This analysis assumes that a liner is placed in the borehole to prevent pore fluid from entering the rock. In the case of an unlined saturated sample, a tension fracture will grow unstably for any crack length. In experiment 2 the borehole was not lined in order that pore fluid could diffuse into the previously dry rock, resulting in a partially saturated sample at the time of failure. In this case, viscosity of the pore fluid may control the rate at which it can flow to the fracture front, producing a period of quasi-stable crack growth.

Even though the region around the borehole was at a very low effective pressure and high differential stress for more than an hour before failure, it did not fail locally in shear. This suggests that, locally, the strength of rock is a function not only of stress but also of stress gradients [*Jaeger*, 1967], a parameter that should be studied in more detail. It may be that the microfractures occurring during the early stable part of the failure sequence were indeed the result of small-scale shearing of the region of low effective pressure prior to the development of a well-defined tension fracture. In experiment 1 the stress supported by the sample dropped considerably prior to failure, indicating extensive crack development. This occurred without producing acoustic emission above the threshold sensitivity of our experiment. It is possible that cracking of this nature occurred in experiment 2 in the region of high pore pressure about the borehole. If this is so, this region would be supported by the surrounding intact rock. The understanding of how small-scale crack growth develops into macroscopic failure has been a long-standing problem in rock mechanics. Because of this, little more can be said of the precise mechanism that led to macroscopic failure in these samples.

In the literature on hydraulic fracture the possibility of producing shear rather than tension fractures is surprisingly disregarded. The results presented in this paper show that in the laboratory it is a simple matter to control the type of fracture produced. Hydraulic fracturing performed in situ, particularly in regions of large tectonic stress, might be done in ways that could produce either shear or tension fractures. One case in which shear fractures were induced by hydrofracturing occurred when waste fluids were disposed of at the Rocky Mountain Arsenal by injecting them into the basement rock. Analysis of resultant earthquakes by *Healy et al.* [1968] showed that fractures formed in shear. *Raleigh et al.* [1972] have shown that hydrofrac experiments conducted at Rangely, Colorado, resulted in fracturing along a previously existing fault zone. This suggests that in regions where deviatory tectonic stress is not large enough to initiate shear cracks, failure could still occur in shear by remobilizing preexisting faults. For example, the most common theoretical models used to relate breakdown pressure to regional stresses [*Hubbert and Willis*, 1957] suggest that the breakdown pressure is a unique function of the principal stresses, the tensile strength of the rock, and the pore pressure. Because this analysis assumes that a tension fracture will form, the model would not be applicable for a rock that failed in shear. All of the experiments shown in Figures 2 and 9 were conducted under the same principal stresses, and yet those samples failing in shear had lower breakdown pressures than those failing in tension. Figure 10 shows the borehole pressure curves for four experiments in which pore fluid was injected at the same rate. The normal interpretation of this data would be that the samples failing at higher pressures were under higher stress when in fact just the opposite is the case. The samples subjected to the highest differential stress failed in shear at low injection pressures before the pore pressure could increase to the point where they would fail in tension.

Another problem arises in that shear and tension fractures will propagate in different directions. In hot rock geothermal models, for example, it is proposed that a fracture be formed that will later be intersected by a well some distance from the injection well. If a shear fracture were formed unintentionally in such a project, the second well might miss the fracture zone completely.

These experiments suggest that simply by varying the injection rate, either tension or shear fractures could be formed in situ when regional stresses are favorable. This would provide flexibility in selecting a fracture orientation more suited for particular needs.

Controlling of fracture type by the rate of fluid injection could have an application in the generation of artificial geothermal reservoirs where it is desirable to generate the largest amount of fracture surface area in a given volume of rock. Since producing a single tension or shear fracture would create only one surface along which to heat a circulating fluid, heat exchange would be inefficient. If, however, one were to inject fluid into the rock rapidly, causing a tension fracture, and then

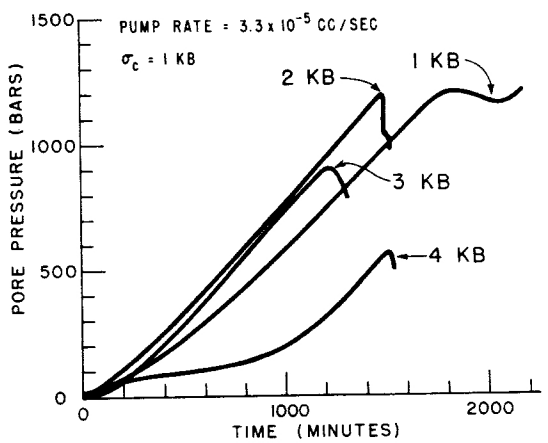

Fig. 10. Borehole pressure curves for four experiments conducted at 1-kbar confining pressure and an injection rate of 3.3 × 10^{-5} cc/s. Differential stress ranged from 1 to 4 kbar.

maintain the pore pressure just below what would be required to further extend the fracture, one or more shear fractures should soon propagate off the primary fracture. In this way, the fracture surface area in the rock could be augmented manyfold. We have successfully generated such composite fractures in the laboratory. At high differential stress and high injection rates, samples developed tension fractures with no accompanying axial strain. Within seconds, however, they failed in shear. The benefits of being able to create such fracture systems warrant further investigation in the field.

The most critical results of these experiments are as follows. (1) We have demonstrated that in controlled laboratory conditions we are able to trace the development of hydraulically induced fractures by monitoring the acoustic emission generated during fracturing. (2) We have demonstrated that hydrofracturing can generate shear fractures rather than tension fractures, depending on the regional stresses, injection rate, and rock permeability. (3) For suitable regional stresses, either shear or tension fractures can be generated simply by varying the rate at which fluid is injected into the rock. (4) Theoretical calculations of the pore pressure distribution in the samples at failure support the hypothesis that the failure mode is controlled by the distribution of effective pressure in the rock.

All of these results have important implications in field hydraulic fracture projects. They suggest that we ought to have a closer look at some of the long-standing assumptions used to interpret borehole pressure data. These assumptions were justified at the time of their conception because they led to the development of a simple and functional model that was in agreement with the limited amount of data available. However, such assumptions should not be immune to reevaluation in light of new results.

REFERENCES

Brace, W. F., J. B. Walsh, and W. T. Frangos, Permeability of granite under high pressure, *J. Geophys. Res.*, *73*(6), 2225–2236, 1968.

Byerlee, J. D., The fracture strength and frictional strength of Weber sandstone, *Int. J. Rock Mech. Min. Sci. Geomech. Abstr.*, *12*, 1–4, 1975.

Byerlee, J. D., and D. Lockner, Acoustic emission during fluid injection into rock, Proceedings of the 1st Conference on Acoustic Emission in Geologic Structures and Materials, Trans Tech Publications, Clausthal-Zellerfeld, West Germany, in press, 1977.

Clifton, R. J., E. R. Simonson, A. H. Jones, and S. J. Green, An application of linear elastic fracture mechanics to pressurized thick walled vessels, Terra Tek, Inc., Salt Lake City, Utah, 1974.

Clifton, R. J., E. R. Simonson, A. H. Jones, and S. J. Green, Determination of the critical stress-intensity factor K_{1c} from internally-pressured thick-walled vessels, *Exp. Mech.*, *16*(6), 233–238, 1976.

Healy, J. H., W. W. Rubey, D. T. Griggs, and C. B. Raleigh, The Denver earthquakes, *Science*, *1*, 1301–1310, 1968.

Hubbert, M. K., and D. G. Willis, Mechanics of hydraulic fracturing, *Trans. AIME*, *210*, 153–168, 1957.

Jaeger, J. C., Brittle fracture in rocks, in *Failure and Breakage of Rocks*, pp. 3–7, Port City Press, Baltimore, Md., 1967.

Mathews, C. S., and D. G. Russel, Pressure buildup and flow tests in wells, *Soc. Petrol. Eng. J.*, *1*, 1–167, 1967.

Raleigh, C. B., J. H. Healy, and J. D. Bredehoeft, Faulting and crustal stress at Rangely, Colorado, in *Flow and Fracture of Rocks*, *Geophys. Monogr. Ser.*, vol. 16, edited by H. C. Heard et al., AGU, Washington, D. C., 1972.

Sanyal, S. K., R. M. Pirnie III, G. O. Chen, and S. S. Marsden, Jr., A novel liquid parameter for measuring very low permeability, *Soc. Petrol. Eng. J.*, *12*(3), 206–210, 1972.

Shuck, L. A., and T. W. Keech, Monitoring acoustic emission from propagating fractures in petroleum reservoir rocks, Penn. State Univ., University Park, 1975.

Shell International Petroleum, *Technical Data on Shell Tellus Oils*, 2nd ed., pp. 20, 50, London, 1967.

Wawersik, W. R., and W. F. Brace, Post-failure behavior of a granite and diabase, *Rock Mech.*, *3*, 61–85, 1971.

Woullet, G. M., and D. V. Power, A seismic study of a large hydraulic fracturing experiment in Wyoming, Abstracts From the First International Symposium on Induced Seismicity, Banff, Alta., Can., 1975.

Yilmaz, O., and A. Nur, Pore pressure fronts in rocks with large permeability moduli (abstract), *Eos Trans. AGU*, *52*, 917, 1971.

Zoback, M. D., High pressure deformation and fluid flow in sandstone, granite, and granular materials, Ph.D. thesis, Dep. of Geophys., Stanford Univ., Stanford, Calif., 1975.

(Received May 11, 1976;
revised February 8, 1977;
accepted February 9, 1977.)